Rev. Roum. Sci. Techn.– Électrotechn. et Énerg.
Vol. **63**, *4*, pp. 403–409, Bucarest, 2018

Automatique et ordinateurs

SPEED SENSORLESS VECTOR CONTROL OF INDUCTION MOTOR USING ONLINE NEURAL VOLTAGE-CURRENT PHASE DIFFERENCE ESTIMATION

RABIE SAIFI[1], NASREDINNE NAIT-SAID[1], ABDESSALAM MAKOUF[1], LARBI CHRIFI-ALAOUI[2], SAID DRID[1]

Key words: Induction motor, Speed sensorless, Neural network, Vector control.

This paper aims to describe a speed sensorless control of induction motor (IM) based on a new neural network estimator of the rotor speed. This method is based on the extraction of the rotor speed information from the command frequency and the phase difference between stator current and voltage. The data used to train the artificial neural network (ANN) are obtained from steady state equivalent circuit of the induction motor simulated for various frequency. The experimental results show the efficiency of the proposed speed estimation technique at high speed and at very low speed.

1. INTRODUCTION

In order to realize an efficient speed control of induction motor, speed sensors, such as encoder, resolver or tachometer may be utilized. However, some problems appear such as, need of shaft extension, which decreases the mechanical robustness of the drive, reduce the reliability, and increase in cost [1–5]. The elimination of speed sensors without losing performances has constituted a very important field of research works [6]. Several solutions to solve this problem have been suggested. Based on the motor fundamental excitation model, high frequency signal injection methods have been proposed in [7]. The necessity of external hardware for signal injection and the adverse influence of injecting signal on the motor performance [8–10] do not constitute an advantage for this technique. Fundamental model-based strategies method using instantaneous values of stator voltages and currents to estimate the rotor speed has been investigate. Several other methods have been proposed, such as model reference adaptive system (MRAS) sliding mode observers, *Luenberger* observer and *Kalman* filter. Recently speed sensorless method based on artificial intelligence techniques, such as fuzzy logic and artificial neural network have been developed [9,10].

The main problems of these models based estimators are their sensitivity to a parameters change and their low performances at very low and zero speed.

In consequence all problems cited above lead to a category of estimator which are insensitive to a parameters change, requiring small design effort and increasing capacity for a good estimation. The artificial intelligence has been known as a robust tool susceptible to simulate a nonlinear system with any desired degree of accuracy [10–13]. Several artificial neural networks have been proposed in the sensorless speed control of the induction motors IM.

In this paper we present a sensorless speed control of the induction motor using an artificial neural network (ANN), based mainly on the command frequency f and the phase difference θ between stator voltage and current. The principle of speed estimator and the control system scheme are described in the following. Experimental results are also presented to demonstrate the effectiveness and performance of the proposed method.

2. PRINCIPLE

In the upper speed range above a few hertz stator frequency, the resistive voltage $R_S{\cdot}i_S$ is small as compared with the stator voltage V_S of the motor, and the estimation of speed can be performed with good accuracy. Even the temperature-dependent variations of the stator resistance are negligible at higher speed. As the stator frequency reduces at lower speed, the stator voltage reduces almost in direct proportion, while the resistive voltage $R_S{\cdot}i_S$ maintains its order of magnitude. It becomes the significant term at low speed. So, the use of the equivalent steady state circuit will lead to large errors in low speed estimation. So, for high frequencies, the phase difference and speed can be calculated for several frequency values, (from 60 Hz to 20 Hz), using the equivalent circuit of an induction motor given in Fig 1. but for low and very low frequencies, using the complex d,q model of induction motor in MATLAB Simulink, (from 18 Hz to 0.5 Hz). The induction motor model in steady state regime can be represented as following [13]:

$$\bar{V}_S = \left(R_S + \mathrm{j}L_S\omega_S\right).\bar{i}_S + \mathrm{j}L_m\omega_S.\bar{i}_R \tag{1}$$

$$0 = \left(R_R + \mathrm{j}L_R\omega_R\right).\bar{i}_R + \mathrm{j}L_m\omega_R.\bar{i}_S, \tag{2}$$

where $\bar{V}_S$ and $\bar{i}_S$ are the stator voltage and current vector, respectively; $\bar{i}_R$ is the rotor current; R_S and R_R are the stator and rotor resistance respectively; L_S , L_R and L_m are the stator, rotor and mutual inductance respectively; ω_S is the electrical angular velocity; ω_R is the rotor speed with $\omega_R = \omega_S - \omega_{sl} = s.\omega_S$, where, ω_{sl} and **s** are the slip angular speed and slip respectively. Thus (2) can be rewritten as:

$$0 = \left(\frac{R_R}{s} + \mathrm{j}L_R\omega_S\right).\bar{i}_R + \mathrm{j}L_M\omega_S.\bar{i}_S \tag{3}$$

To bring back the rotor parameters to the stator side the induction motor model can be rewritten as following:

$$\bar{V}_S = \left(R_S + \mathrm{j}.L_{\sigma s}\omega_S\right).\bar{i}_S + \mathrm{j}L'_m\omega_S.\bar{i}_\mu \tag{4}$$

$$0 = \left(\frac{R'_R}{s} + \mathrm{j}.L'_{\sigma r}\omega_S\right).\bar{i}'_R + \mathrm{j}L'_m\omega_S.\bar{i}_\mu, \tag{5}$$

$$\begin{aligned} L_{\sigma s} &= L_S - L'_m \\ L'_{\sigma r} &= L'_R - L'_m, \end{aligned} \tag{6}$$

[1] University of Batna 2, Laboratory of Induction-Propulsion Systems (LSP-IE), Electrical Engineering Dept, 05000 Batna, Algeria, E-mail: saifi_rabie@yahoo.fr, n.naitsaid@univ-batna2.dz, a_makouf@yahoo.fr, saiddrid@ieee.org
[2] University of Picardie Jules Verne, LTI (EA, 3899), 13 ave. François Mittd., 02880 Cuffies, France, E-mail: larbi.alaoui@u-picardie.fr

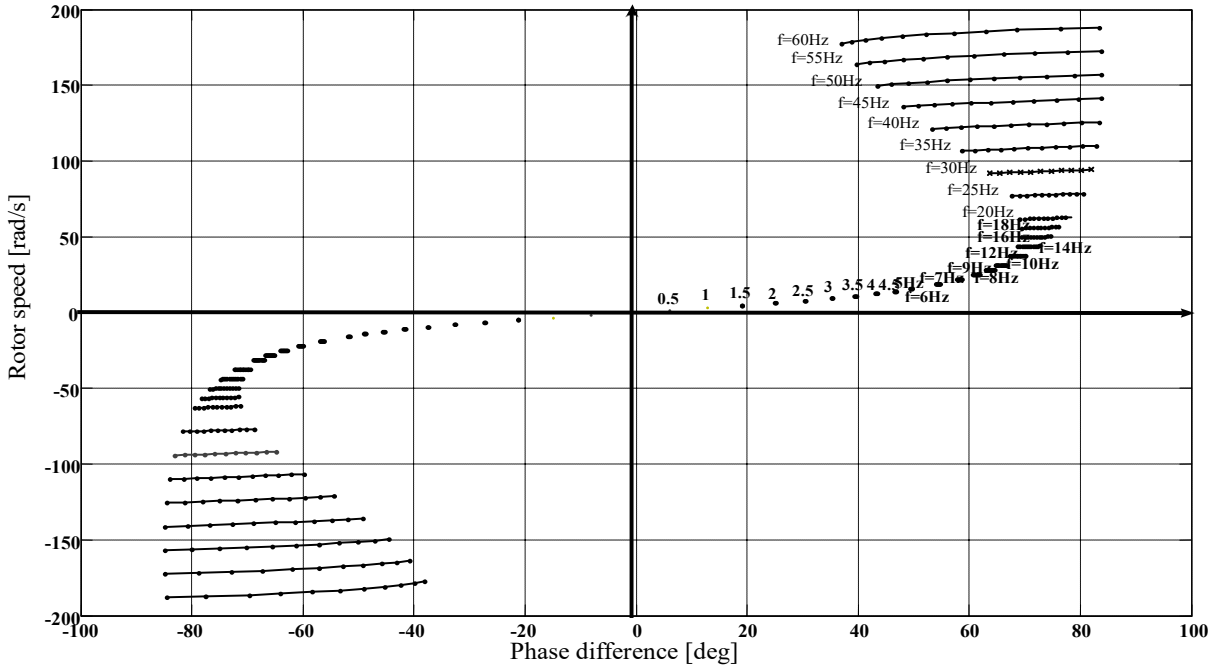

Fig. 2 – Relationship between phase difference and rotor speed, for several command frequency.

$L_{\sigma s}, L'_{\sigma r}$ are the leakage inductances on the side of stator and rotor respectively.

$$L'_m = \chi L_m \tag{7}$$

$$\bar{i}'_R = \frac{\bar{i}_R}{\chi}, \tag{8}$$

$$R'_R = \chi^2 R_R \tag{9}$$

$$L'_R = \chi^2 L_R , \tag{10}$$

where χ is the transformation ratio given by $\chi = \frac{L_m}{L_R}$.

For our case, we consider the total leakage inductance in the stator winding. Adequate transformation taking into account the leakage factor σ [2] leads to an equivalent circuit of induction motor as it is shown by Fig.1:

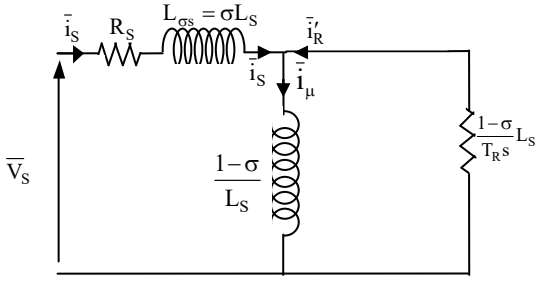

Fig. 1 – T-type equivalent circuit.

The magnetizing current i_μ is obtained by:

$$\bar{i}_\mu = \bar{i}_S + \bar{i}'_R \tag{11}$$

The input impedance is given by:

$$\bar{Z}_{eq} = R_S + \frac{(1-\sigma)L_S\omega_S^2 s T_R}{1+s^2T_R^2\omega_S^2} + j\left(\sigma L_S\omega_S + \frac{(1-\sigma)L_S\omega_S}{1+s^2T_R^2\omega_S^2}\right), \tag{12}$$

where σ is leakage factor

If the previous relation is considered, the phase difference between current and stator voltage can be deduced as follows:

$$\theta = \cos^{-1}\frac{\mathrm{Re}\left[\bar{Z}_{eq}\right]}{\left|\bar{Z}_{eq}\right|}. \tag{13}$$

Figure 2 shows the relationship between θ and ω_R the rotor speed for several stator frequencies values ω_S.

To build the trajectory corresponding to a fixed frequency, we vary the slip between 0 and 100 % to simulate all operating load of the induction motor, and then we compute every time the input impedance. Finally we deduce the phase difference using equation (13). The frequencies vary firstly from 60 Hz to 20 Hz with a step of 5 Hz, in this case, using the equivalent circuit of an induction motor, secondly from 20 Hz to 10 Hz with a step of 2 Hz, thirdly from 10 Hz to 5 Hz with a step of 1 Hz and in the fourth interval from 5 Hz to 0.5 Hz with a step of 0.5 Hz, in the last three cases, using the complex d,q model of induction motor. These characteristics can be obtained in advance by simulation if parameters are known or experimentally and stocked in a database. In this work, the rotor speed is estimated for any frequencies using an ANN. So to train this network, the database cited above contains just twenty six command frequency values. From these relationships, it appears that for a given phase difference and frequency, the rotor speed can be estimated with a great accuracy even in low speed case.

3. NEURAL NETWORK

The training data consists of inputs (frequency and phase difference) and target (rotor speed) obtained from the induction motor equivalent circuit and the complex d,q model of induction motor. A supervised ANN is then trained to produce a desired rotor speed. Its implementation is carried out in two steps. In the first step, a set of 1782 inputs–desired output training data are obtained from simulation of the induction motor model. The speed is deduced from an equivalent circuit of the induction motor and the complex d,q model of induction motor. Obviously,

the two neural networks inputs and the desired output are normalized. To improve the learning operation, the input data to the ANN are subject of polynomial interpolation. This process is iterative for the all learning data considering that every new learning starts from the weights calculated in the former learning operation. During training operation, the ANN program stops when the error value is lower than a goal error one.

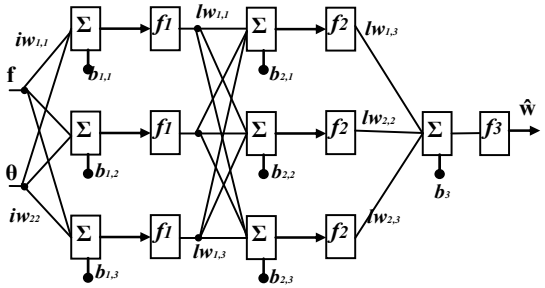

Fig. 3 – Artificial neural network structure.

The second step is involved to test the validity of the trained ANN given by Fig. 3. To test the performance of the speed estimator we use data which are different than the learning ones.

4. SENSORLESS CONTROL

Figure 4 shows the scheme used to determine the frequency f and phase difference θ. θ is obtained by detecting the phase difference between the components of both vector i and vector v on d-q axis while f is deduced from the synchronous angular velocity ω_s of the reference frame (d, q)

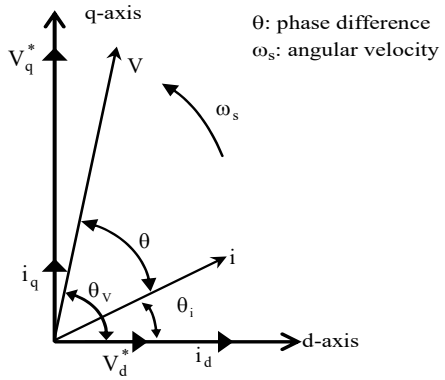

Fig. 4 – Instantaneous phase difference between voltage and current vectors.

θ and f are calculated using the following equations:

$$\theta_V = \tan^{-1}\left(\frac{V_q^*}{V_d^*}\right) \quad (14)$$

$$\theta_i = \tan^{-1}\left(\frac{i_q}{i_d}\right) \quad (15)$$

$$\theta = \theta_V - \theta_i \quad (16)$$

$$f = \frac{\omega_s}{2\pi} \quad (17)$$

Figure 5 shows a block diagram scheme of the ANN based speed sensorless vector control of induction motor.

5. EXPERIMENTAL SETUP

Figures 6 and 7 show the experimental setup of the proposed structure control scheme. The induction motor where the parameters are listed in Table 1 is fed by a three-phase power width modulation (PWM) controlled inverter (4 kW, IGBT modules) from the DS1104 board with TMS320F240 as a slave processor. The dead time and the switching frequency are chosen 5 μs and 10 kHz respectively. The mechanical speed is measured by an incremental encoder. The currents and the voltages are measured by LA-55NP and LV-25P sensors, respectively.

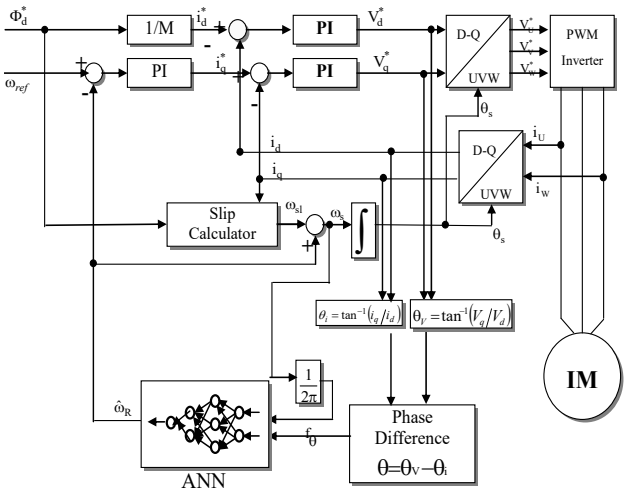

Fig. 5 – Block diagram of the artificial neural network based speed sensorless indirect vector control of IM scheme.

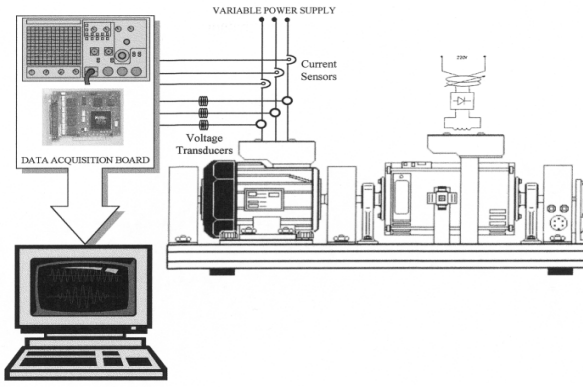

Fig. 6 – Structure of the experimental setup.

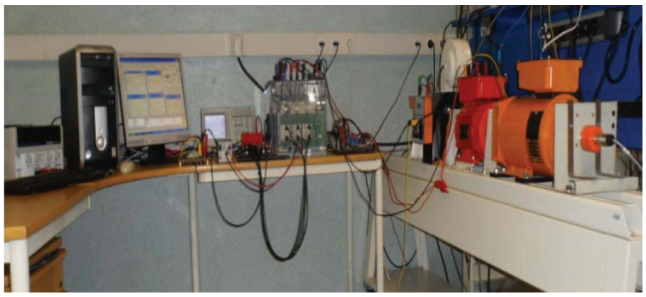

Fig. 7 – Experimental setup in the L.T.I laboratory (Picardie University).

Table 1

Parameter	Value
Rated power	P = 1 KW
Rated voltage	V = 220/380 V
Rated speed	N = 1430 rpm

Number of pole pairs	$p = 2$
Frequency	$f = 50$ Hz
Stator resistance	$R_S = 5.72\ \Omega$
Rotor resistance	$R_R = 4.20\ \Omega$
Stator inductance	$L_S = 0.4621$ H
Rotor inductance	$L_R = 0.4620$ H
Mutual inductance	$L_m = 0.4402$ H
Moment of inertia	$J = 0.0049$ kg/m²
Friction coefficient	$F = 0.003$ N.m.s/rad

6. EXPERIMENTAL RESULTS

To comment results, it is important to note that, for comparison with the estimated speed in the drive scheme control, an incremental encoder measures the real rotor speed. Selected experimental results tests are shown in the following section.

6.1 Test 01–Ramp response with effect loading.

The estimated speed and the "measured" one track the reference profile as observed in Figs. 8 a. Figs. 8 c and 8d show that the tracking speed error (between estimated and reference speed) and the speed estimation error (between estimated and actual speed) are negligible even at zero speed regime and converge rapidly to zero especially in the steady state regime. To test the efficiency and the robustness, a step load torque of 8 Nm is applied with respect to a profile given by Fig. 8 e, from $t = 3.5$ s to $t = 8$ s and between $t = 18$ s and $t = 23.5$ s. As we can see from Fig. 8 b, the flux and torque are still decoupled, since the change in I_{sq} (q axis stator current) does not affect significantly I_{sd} (d axis stator current). The stator current increase respecting load torque variation as observed in Fig 8 f.

6.2 Test 02–Stair-case speed variation from 100 rad/s to 0 and –100 rad/s.

As shown in Fig. 9, the speed varies from 100 rad/s to zero through five steps (100 rad/s, 60 rad/s, 30 rad/s, 5 rad/s and 0 rad/s) an finally continuing to −100 rad/s. Figure 9a shows simultaneously the reference profile, the estimated and measured speed value. It can be observed that the measured and estimated speed closely track the reference speed. One can see also that the I_{sq} stator current component is affected by speed variation with no significant changes on the direct stator current component I_{sd} of the motor as shown in Figs. 9b. Figures 9c and 9d show clearly that the tracking and estimated errors are very small especially in the steady state regime. This test confirms the efficiency and robustness of the proposed scheme control.

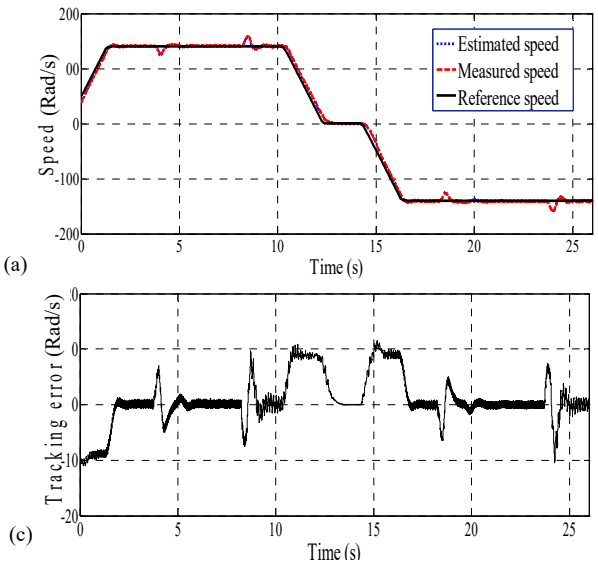

6.3 Test 03–Speed from 30 rad/s to –30 rad /s afterwards it is stopped at 20 % load.

To valid speed estimator at low and zero speed when the motor is under load. The performance of this test is shown in Fig. 10. Measured and estimated speed converge to the reference speed and achieve better speed tracking with a good reject of the load torque perturbations at low and zero speed as shown in Fig.10 a. Fig. 10 b shows that the I_{sd} current is still at constant value. Fig. 10 c and 10 d, present respectively speed estimation error and speed tracking error which are totally negligible and converge rapidly to zero especially in the steady state and at zero speed regime. This test shows and confirms the efficiency and the robustness of the proposed neural network based speed estimator even at low and zero speed.

6.4 Test 04–Take off from zero speed to 10 rad/s after 5 s at 20 % load.

In this case, the drive efficiency is checked to maintain decoupled the magnetization flux and the torque at zero speed followed by enforcement to a fixed reference speed. This test is shown in Fig.11. Measured and estimated speed closely track the reference speed under load torque disturbance at very low and zero speed as observed in Fig.11 a. We can see changes in I_{sq} (q axis stator current) and no change affecting significantly I_{sd} (d axis stator current) throughout the motor operation as shown in Fig.11 b.

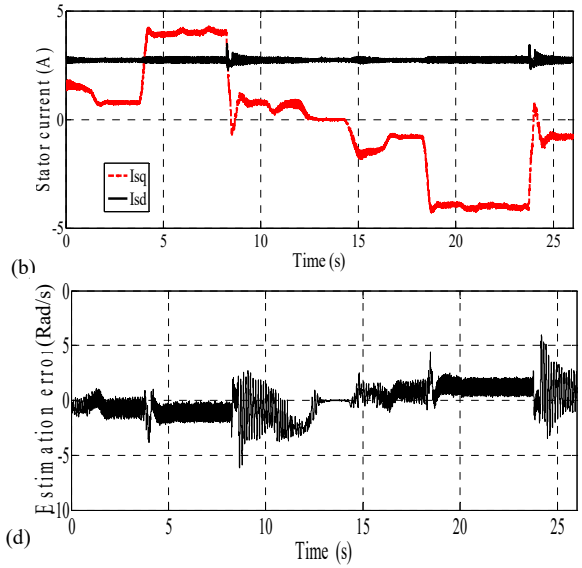

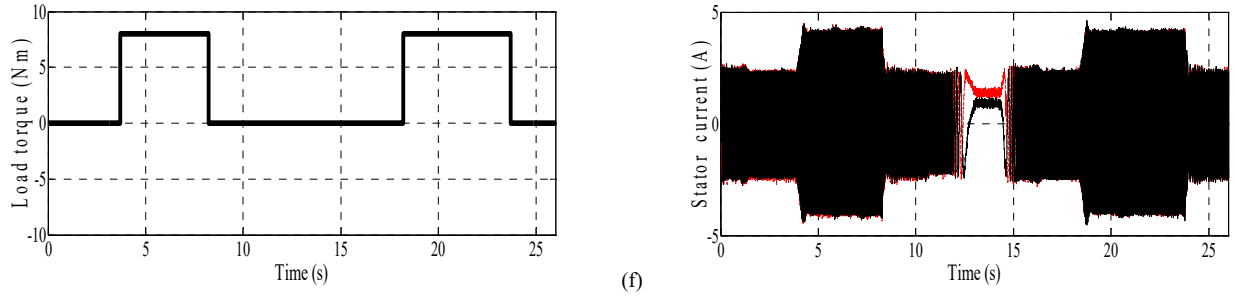

(e) (f)

Fig. – 8 Dynamic responses of rotor speed inversion from ω_{ref} = 140 rad/s to ω_{ref} = −140 rad/s under 100 % load torque T_L = 8 Nm.

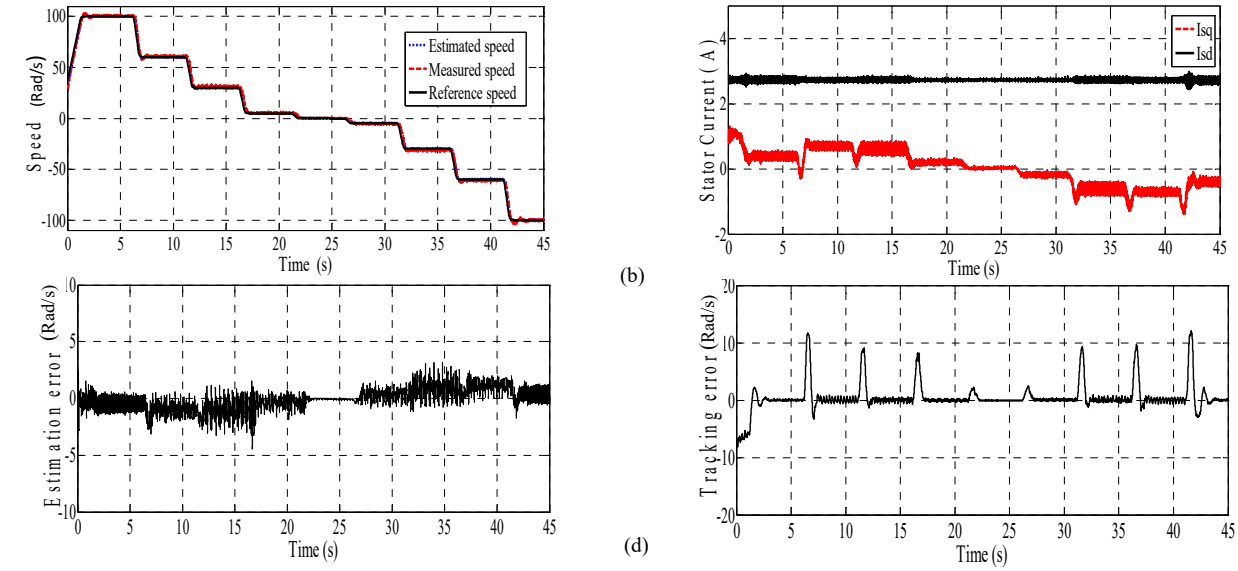

a) (b) (c) (d)

Fig. 9 – Dynamic responses of stair case rotor speed transient from ω_{ref}= 100 rad/s to ω_{ref} = −100 rad/s at no load torque.

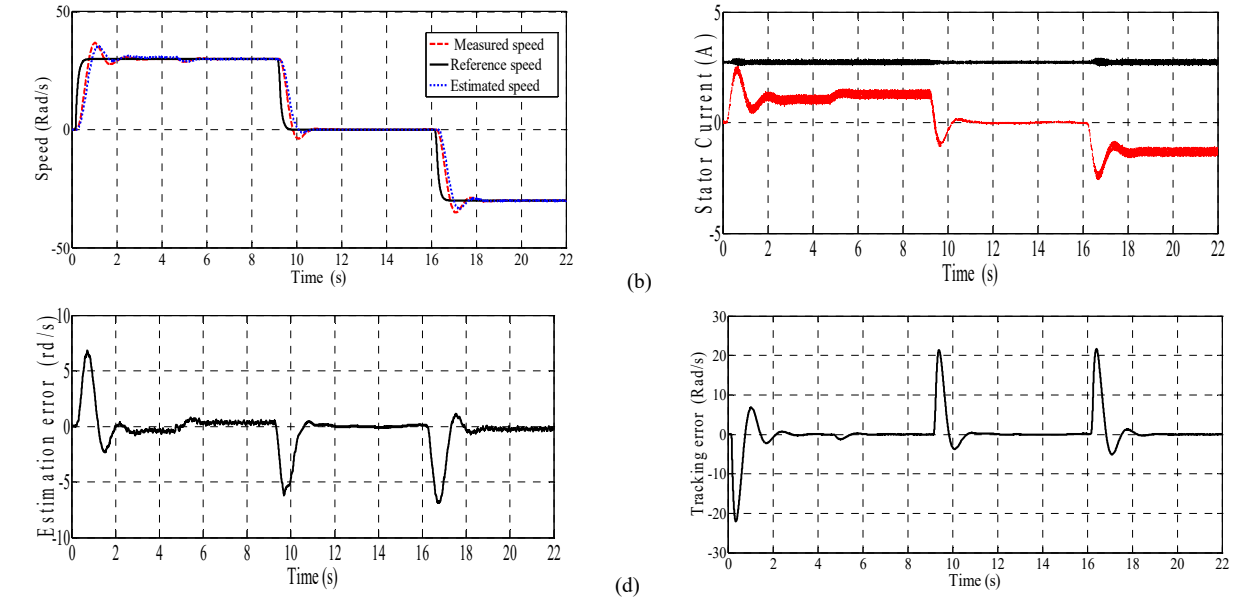

(a) (b) (c) (d)

Fig. 10 –Dynamic responses of low speed inversion from ω_{ref}= 30 rad/s to ω_{ref} = −30 rad/s afterwards it is stopped, at 20 % load torque rejection at t = 5 s.

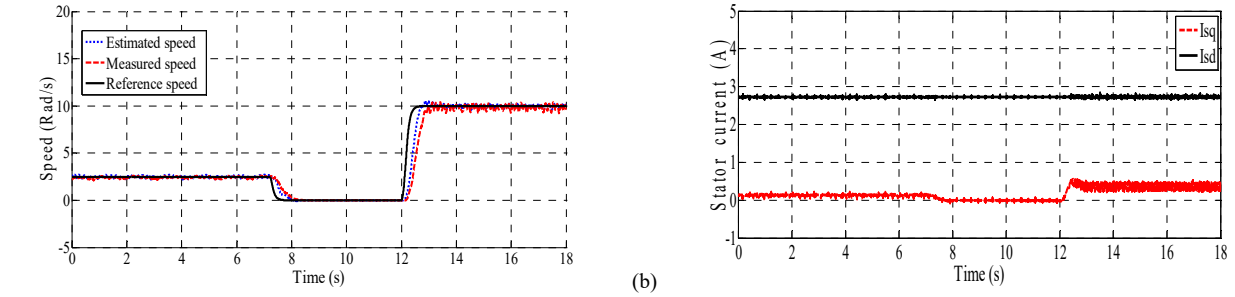

(a) (b)

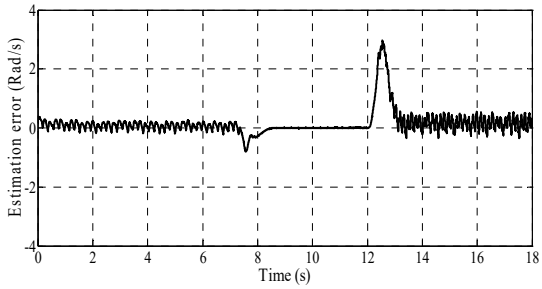

(c)

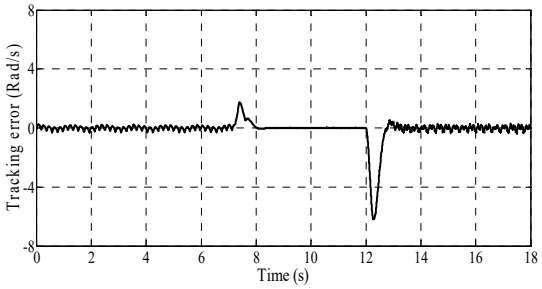

d)

Fig. 11 – Dynamic responses of take from zero speed to 10 rad/s, at 20 % load.

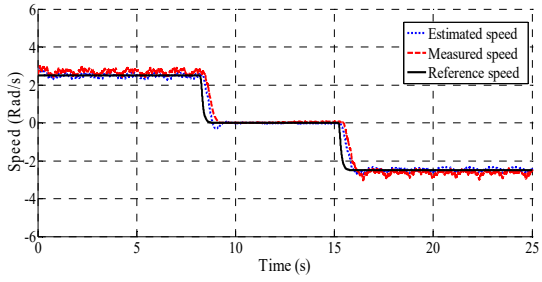

(a)

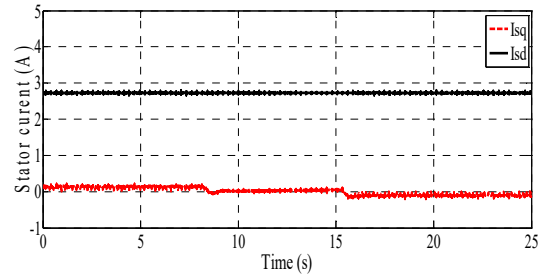

(b)

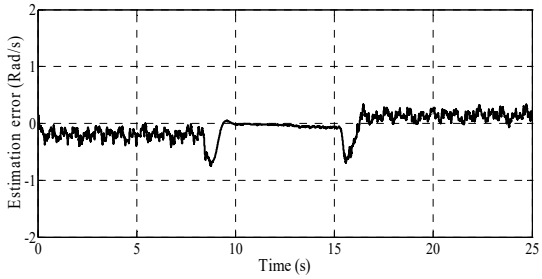

(c)

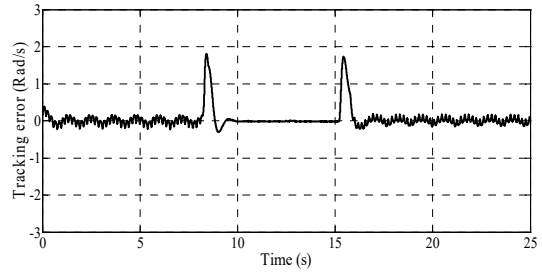

(d)

Fig. 12 – Dynamic responses of very low speed inversion from ω_{ref} =2.5 rad/s to ω_{ref} = −2.5 rad/s afterwards it is stopped, at 15 % load torque rejection at t = 5 s.

Also, after weak variations, tracking and estimation speed errors converge rapidly to zero especially in the steady state regime as observed in Fig.11c and Fig.11 d.

6.5 Test 05– ±2.5 rad/s speed reversal afterwards it is stopped at 10% load.

The performance of the proposed speed sensorless control, at very low and zero speed when the motor under load torque is shown in Fig. 12. The measured and estimated speed closely track the reference profile as observed in Fig. 12 a. The decoupling between I_{sd} (d axis stator current) and I_{sq} (q axis stator current) is observed in Fig.12 b. We can see that the profile of the stator current component I_{sq} has changed with the motor speed while the stator current component I_{sd} is constant throughout the motor operation. The sensorless control presents better steady state and dynamic performance with negligible steady state error between the estimated, measured and reference speeds particularly around zero speed, as it is shown by Figs. 12 c and 12 d.

The experimental results confirm that high performances are obtained with the proposed speed sensorless indirect field-oriented control method.

7. CONCLUSION

In this paper, a new method using an artificial neural network based speed estimator is performed for speed sensorless control of an induction motor using stator frequency and phase difference between stator voltage and current**.** The training of the ANN has been done from data obtained using equivalent circuit model of an IM in steady state regime.

The experimental results obtained confirm the improvement brought with the proposed method, especially at very low and zero speeds.

ACKNOWLEDGMENTS

The authors would like to thank the L.T.I laboratory, Picardie University, Jules Verne (FRANCE), for providing the computing facilities.

Received October 1, 2016

REFERENCES

1. V. Verma, C. Chakraborty, S.Maiti, Y. Hori, *Speed sensorless vector controlled induction motor drive using single current sensor*, *IEEE Trans. Energy Convers.*, **28**, *4*, pp. 938–950, Nov. 2013.
2. R. Verma, V. Verma, C. Chakraborty, *ANN Based Sensorless Vector Controlled Induction Motor Drive Suitable for Four Quadrant Operation*, Proc. of the Students' Technology Symposium, pp. 182–187, 2014.
3. J. Holtz, *Sensorless Control of Induction Machines – With or Without Signal Injection?* IEEE Trans. on Ind. Electronics, **53**, *1*, pp. 07–30, Feb. 2006.
4. J. Holtz, *Drift- and Parameter-Compensated Flux Estimator for Persistent Zero-Stator-Frequency Operation of Sensorless-Controlled Induction Motors*, IEEE Trans. on Ind. Applications, **39**, *4*, pp. 1060–30, Jul/Aug. 2003.
5. H. Feroura, F. Krim, B. Talbi, A. Laib, A. Belaout, *Sensorless Field Oriented Control of Current Source Inverter Fed Induction Motor Drive*, Rev. Roum. Sci. Techn. – Électrotechn. et Énerg., **63**, *1*, pp.100–105, 2018.

6. Y. Oguz, M. Dede, *Speed estimation of vector controlled squirrel cage asynchronous motor with artificial neural networks ScienceDirect*, Energy Convers. and Manag., **52,** pp. 675–686, 2010.
7. S. M. Gadoue, D. Giaouris, W. Finch, *Sensorless Control of Induction Motor Drives at Very Low and Zero Speeds UsingNeural Network Flux Observers*, IEEE Trans. on Indus. Electronics, **56**, *8*, pp. 3029-3039, 2009.
8. C. Lascu, I. Boldea, F.Blaabjerg, *Very-Low-Speed Variable-Structure Control of Sensorless Induction Machine Drives Without Signal Injection*, IEEE Trans. on Indus. Applications, **41**, *2*, pp.591–598, 2005.
9. I. Benlaloui, S. Drid, L. Chrifi-Alaoui, M. Ouriagli, *Implementation of a New MRAS Speed SensorlessVector Control of Induction Machine*, IEEE Trans. on Energy Conv.,**30**, *2*, pp. 588–595, 2015.
10. C. Caruana, G.M. Asher, M. Sumner, *Performance of high frequency signal injection techniques for zero-low-frequency vector control induction machines under sensorless conditions*, IEEE Trans. Ind. Electron.**, 53**, *1*, pp. 225–238, 2006.
11. E. Benyoussef, A. Meroufel, S. Barkat, *Neural Network and Fuzzy Logic Direct Torque Control of Sensorless Double Star Synchronous Machine*, Rev. Roum. Sci. Techn. – Électrotechn. et Énerg., **61**, *3*, pp.239–248, 2016.
12. M. Kuchar, P. Brandstetter, M. Kaduch, *Sensorless Induction Motor Drive with Neural Network*, IEEE Power Electronics Specialists Conference, pp. 3301-3305, 2014.
13. Z. Aydogmus, O. Aydogmus, *A comparison of artificial neural network and extended Kalman filter based sensorless speed estimation*, ScienceDirect, Measurement, **63**, pp. 152–158, 2014.